Pol. J. Environ. Stud. Vol. XX, No. X (XXXX), 1-17
DOI: *10.15244/pjoes/240372* ONLINE PUBLICATION DATE: 2026-11-26

Original Research

Genesis Mechanism of the Huitang Geothermal Field in Hunan Based on Hydrochemical and Isotopic Characteristics

Yao Peng[1, 2], Hui Tian[3]*, Hengtai Chen[4], Changhui Li[2], Liangliang Dai[2], Huang Zhang[2], Kun Luo[2], Fuchao Li[2], Zhou Ouyang[2], Huijiao He[4]

[1]Chinese Academy of Geological Sciences, Beijing 100037, China
[2]Changsha General Survey of Natural Resources Center, China Geological Survey, Ningxiang 410600, China
[3]Department of Water Science and Engineering, Hunan University of Technology, Zhuzhou 412007, China
[4]Ningxiang Cultural Tourism Investment Co., Ltd., Ningxiang 410600, China

Received: 30 January 2026
Accepted: 27 September 2026

Abstract

The Huitang geothermal area is a significant geothermal resource zone in Hunan Province. Understanding its formation processes is crucial for geothermal development. The study explores the genesis of the Huitang geothermal field. Hydrochemical and isotopic analyses of geothermal and cold waters provide the basis for the interpretation. Two primary heat sources are identified: terrestrial heat flow contributes to the thermal input, while radioactive decay in granite provides additional heat. Calculations using the SiO_2 geothermal temperature scale yield reservoir temperatures ranging from 135.69ºC to 140.98ºC. However, the mixing of cold water leads to an underestimation of these values. Therefore, corrections are required using the silicic acid diagram method. Hydrogen and oxygen isotope analysis reveals lateral recharge originating from higher-elevation terrain to the west. The inferred recharge elevations range from 443.84 to 493.67 m, and the circulation depth is 3411-3562 m. The chemical type of the geothermal water at Huitang is primarily HCO_3^--Na. Gibbs diagram analysis shows that rock alteration dominates hydrothermal-rock interactions. Strontium isotope ($\delta^{87}Sr/\delta^{86}Sr$) signature analysis confirms a significant influence from silicate rock alteration and dissolution. The study integrates these results to propose a geothermal genesis mechanism for the Huitang field.

Keywords: Huitang, geothermal, hydrochemistry, isotopes, genesis mechanism

*e-mail: 359585977@qq.com
0000-0001-9315-1956

© 2026 This article is licensed under a Creative Commons Attribution-NonCommercial 4.0 International (CC BY-NC 4.0)

Introduction

Geothermal resources serve as natural sources of thermal energy. The energy originates from radioactive decay and the conductive transfer of heat within the Earth's interior [1]. China is among the earliest nations to harness geothermal energy. Compared to energy derived from traditional fossil fuels, geothermal energy offers greater abundance, broader distribution, greater resource conservation, reduced emissions, and a stable, continuous supply [2, 3]. Geothermal energy also plays a crucial role in heating, power generation, and industrial thermal applications. According to IGA statistics, China consistently leads the world in annual geothermal utilization across the heating, power generation, and industrial thermal sectors [4]. As global energy demands evolve and clean energy gains prominence, an increasing number of countries are incorporating geothermal resources into their energy mixes.

China possesses abundant geothermal resources, accounting for one-sixth of the world's total. Based on reservoir temperatures, these resources can be categorized into low-to-medium-temperature (25-150ºC) and high-temperature (≥150ºC) geothermal systems. China's geothermal resources are predominantly characterized by low-to-medium-temperature systems [4]. Their spatial distribution is marked by greater resource abundance in the east and west and by higher temperatures in the south than in the north [5]. Key analytical methods for studying geothermal resources currently include hydrothermal water chemistry and isotope analysis. These techniques reveal the environmental conditions, recharge sources, reservoir temperatures, and mechanisms of water-rock interaction in geothermal fluids, thereby elucidating their formation processes. Both domestic and international studies have employed these methods to analyze geothermal waters. For instance, Taylor established the hydrogen-oxygen isotope shift principle to analyze water-rock interactions in hot-water systems [6], identifying distinct sources, such as deep primordial water and atmospheric precipitation recharge. Drawing on geochemical solute equilibrium concepts, Giggenbach proposed the Na–K–Mg diagram. The diagram serves to evaluate the maturity of geothermal waters and to calculate equilibrium temperatures [7]. Minissale et al. integrated gas geochemistry and hydrochemistry to investigate deep geothermal processes [8]. Reservoir temperatures were estimated using geochemical thermometers. In China, Zhou et al. systematically analyzed geothermal waters in Anhui Province using hydrochemical indicators and hydrogen-oxygen isotope ratios, thereby identifying recharge sources and water-rock interaction processes [9]. Shi et al. analyzed the Baijing geothermal system by integrating hydrochemistry, isotopic geochemistry, multi-mineral equilibrium modeling, and the Si-enthalpy method, thereby enabling the identification of system characteristics and the development of a genetic model [10]. For the geothermal waters in northern Jinan, Yin et al. conducted ionic and isotopic analyses to determine their hydrochemical properties, formation mechanisms, recharge origins, and reservoir temperatures, thereby constructing a conceptual model of geothermal circulation [11].

Located along the southern margin of the Chinese continent, the central-southern region of China is characterized by low- to medium-temperature convective geothermal systems and abundant geothermal resources [12]. It has been the subject of extensive research. For example, Li et al. systematically investigated the medium-low-temperature geothermal field in Zhongshan, Guangdong Province, using hydrochemical analysis, H–O isotope tracing, and a silica-enthalpy mixing model. They established a genetic model for the geothermal waters [13]. Liu et al. combined MT/AMT electromagnetic inversion with hydrogeochemical analysis to examine the formation mechanism of the Kahui geothermal field in western Sichuan and, for the first time, identified the Litang Fault and the Kahui Fault as the dominant heat-controlling structures [14]. Huang et al. applied multi-isotope (O–H–Sr–C–He) tracing and ion analysis to water samples collected from the XL and CL fault zones in the Yunkai Uplift, South China, to determine reservoir temperatures, circulation depths, and mixing processes, thereby revealing the genetic model of this region [15].

The Huitang geothermal area is recognized as an essential geothermal zone in Hunan Province. Natural hot springs with temperatures up to 102ºC are exposed at the surface. The area is classified as a high-temperature geothermal field. Previous studies have investigated the Huitang geothermal area based on exploration and analysis. Wan concluded that the Huitang geothermal system is a hydrothermal geothermal field primarily controlled by the combined effects of active faults and the regional structural stress field [16]. Ou et al. used a conduit model to estimate the resource potential of granite hot dry rocks based on geophysical data, terrestrial heat-flow values, granite thermal conductivity, and granite heat-production rates, and the results indicated burial depths of 3.13-3.50 km and 3.84-4.28 km [17]. Previous studies have characterized the geothermal rock body in Huitang. The current study extends this work by identifying the heat and water sources of the geothermal system. Hydrochemical and isotopic data are integrated to assess the geothermal water's hydrochemical characteristics.

This study functions as a valuable reference for investigating the genesis of medium–low-temperature convective geothermal systems and developing geothermal resource assessments. It guides rational exploitation and improves understanding of the formation of fault-controlled geothermal systems. The study promotes the combination of hydrochemistry, isotope geochemistry, and geothermics, advancing geothermal geology. The Huitang geothermal field in Hunan Province was chosen as a representative case.

We systematically collected geothermal water and regional cold water samples from the Huitang geothermal field. Hydrochemical analyses, stable isotope measurements (δD and $\delta^{18}O$), and strontium isotope ($^{87}Sr/^{86}Sr$) measurements were conducted. These were integrated with SiO_2 geothermometry and a silica-enthalpy mixing model. This approach permitted a complete investigation of chemical characteristics, heat-source composition, reservoir temperatures, and mechanisms of water-rock interaction.

The particular objectives of this work are to identify the types of heat sources and their proportions, determine the circulation depth and recharge sources of deep geothermal water, and clarify the genetic model and ascent evolution of the geothermal fluids. The findings supply essential baseline information and theoretical support for the rational development and sustainable use of the Huitang geothermal field. They also serve as a reference for studies of similar geothermal fields in Hunan.

Materials and Methods

Geological and Geothermal Setting

Huitang Town is located within a composite zone of Huaxia System fault structures, including the northern wing reflection arc of the Qiyang Arc. Under the influence of stress sources, varying boundary conditions, and stress transformation, the study area exhibits poorly developed folds, leading to relatively well-developed fault structures. The primary fault structures within the area include the Wujiang Fault (F_1), the Shiqiao Fault (F_2), and the Bamuchong Fault (F_3), as shown in Fig. 1. Among these, the Wujiang Fault, acting as a heat-conducting fault structure, remains active. The primary heat sources in Huitang are distributed within fault zones, such as K10, K11, K12, and K13, within the study area. The fault zones and their associated secondary faults clearly control these sources.

Furthermore, the mechanical characteristics of neotectonic faults influence the formation of geothermal water. Consequently, a series of densely arranged, parallel, northeast-trending streams and rivers has developed near Ningxiang, with numerous steep banks along their southeast shores. Stratigraphic lithology is closely related to the geothermal system [18]. Huitang exhibits relatively simple stratigraphic lithology, with exposed formations including Quaternary Pleistocene deposits dominated by sub-clay and gravel. The Upper Cretaceous Upper Series is composed primarily of strongly weathered granitic, calcareous, and conglomeratic rocks, and Yanshan-period granites, dominated by syenite-biotite porphyry granite and plagioclase-biotite porphyry granite. Among these, the Huitang granite exhibits favorable rock heat generation rates [19], serving as the thermal reservoir for the Huitang geothermal area. The highly weathered granite layers and Cretaceous mudstones, sandstones, and other lithologies exhibit low thermal conductivity, forming the cap rock of the Huitang geothermal area. Deep, large-scale faults developed within the region are connected to high-temperature intrusive bodies at depth, providing excellent thermal conductivity and serving as heat conduits for the Huitang geothermal area.

Sampling and Analysis

This study primarily collected cold and geothermal water from the Huitang area, totaling 29 samples, including 6 geothermal samples. These samples underwent both water chemistry and isotope analyses (Fig. 1). Tests included physicochemical parameters such as pH, electrical conductivity (EC), total dissolved solids (TDS), and total hardness (TH), as well as cations (Na^+, Ca^{2+}, K^+, Mg^{2+}), anions (HCO_3^-, SO_4^{2-}, NO_3^-, Cl^-, CO_3^{2-}, F^-), trace elements (Fe, Mn), metasilicic acid, and stable isotopes (δD, $\delta^{18}O$, and $\delta^{87}Sr/\delta^{86}Sr$). All collected samples were refrigerated at 4ºC and tested within one week. Cations (Na^+, Ca^{2+}, K^+, Mg^{2+}) were analyzed using an inductively coupled plasma spectrometer (iCAP 7400). At the same time, anions (Cl^-, SO_4^{2-}, NO_3^-, F^-) were determined by ion chromatography (CIC-D100), HCO_3^- by hydrochloric acid titration, and metasilicic acid by a multi-parameter water quality analyzer. To ensure accuracy, we kept charge-balance errors within ±5% for most samples and analyzed δD and $\delta^{18}O$ using a water isotope analyzer (LGR, USA, IWA-45EP). Similarly, to ensure analytical reliability, the standard deviation relative to SMOW must be strictly controlled. The acceptable limits are ±2% for δD and ±0.30% for $\delta^{18}O$. We measured the strontium isotope ratio ($^{87}Sr/^{86}Sr$) using thermal-ionization mass spectrometry, with an error of ±0.00006.

Research Methods

Hydrochemistry Analysis

The study uses the box plot, the Piper diagram, and the Gibbs diagrams. The concentration trends of major ions in the water samples were visually analyzed using a multi-factor box plot. A Piper ternary diagram, commonly used to analyze the relative abundance of ions in groundwater and to determine its hydrochemical type, was constructed from ion concentrations. Gibbs diagrams provide a visual representation of the key factors influencing groundwater chemistry.

By analyzing the relationships between TDS and $Na^+/ (Na^+ + Ca^{2+})$, as well as $Cl^-/ (Cl^- + HCO_3^-)$, one can assess the extent to which atmospheric precipitation, rock alteration, and evaporation-concentration processes affect groundwater composition [20].

The CAI-II versus CAI-I diagram is used to evaluate whether cation-exchange responses occur in the groundwater. To investigate the origin of geothermal water chemistry, principal component analysis (PCA)

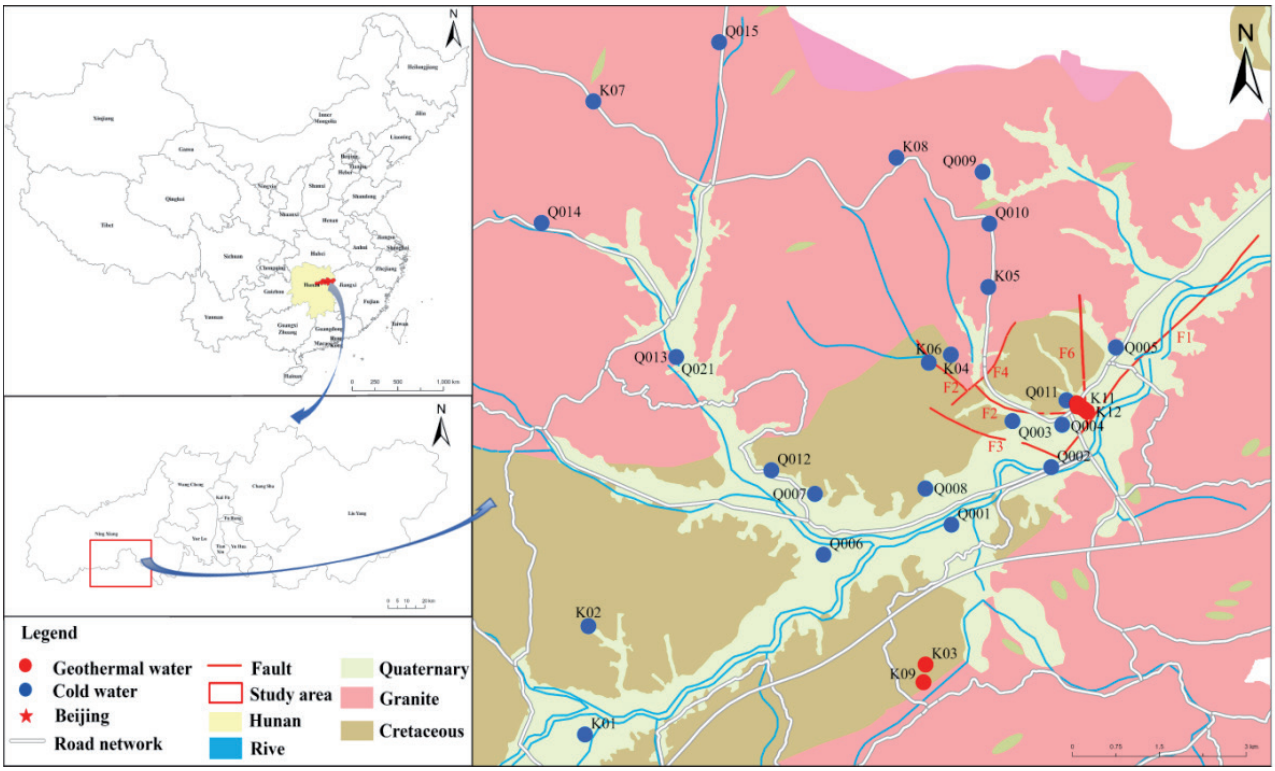


Fig. 1. Spatial distribution of geothermal water sampling points in the Huitang area.

was performed on major water chemistry components (Ca^{2+}, Na^{+}, K^{+}, Mg^{2+}, HCO_3^{-}, SO_4^{2-}, Cl^{-}, TDS) and characteristic components (F^{-}, SiO_2) [21].

Geochemical Calculation

Isotopic End-Member Mixing Model

Geothermal water isotopes are essential for tracing the source, flow, and evolution of geothermal water, as well as for assessing geothermal resources. Their primary applications include identifying the source reservoir of geothermal water, estimating reservoir temperatures, and determining water-rock interactions [22].

Based on the altitude effect on hydrogen and oxygen stable isotopes, the recharge altitude of geothermal water is determined, and groundwater recharge zones are identified (Eq. (1)) [23].

$$H = \frac{(\delta_k - \delta_p)}{K} + h \quad (1)$$

In the formula, δ_k represents the δD value (‰) of the geothermal water, and δ_p denotes the δD value (‰) of local atmospheric precipitation. H refers to the elevation (m) of the geothermal water recharge area. h represents the elevation (m) of the geothermal water sampling point. K is the isotopic elevation gradient (‰/m), representing the decrease in δD per 1-meter increase in elevation. Based on previous data, K is assigned a value of –0.023.

Strontium isotopes ($\delta^{87}Sr/\delta^{86}Sr$) serve as powerful tracers in geochemistry, revealing the source-area properties of hydrothermal fluids, the intensity of water-rock reactions, contributions from deep processes, and the evolution history of mixing. They are key indicators for establishing geothermal system genesis models and for assessing resource potential and environmental risks. They are commonly used to distinguish water-rock interactions of different lithologies. $\delta^{87}Sr/\delta^{86}Sr$ values between 0.716 and 0.720 indicate silicate alteration, while a value of 0.708 indicates carbonate alteration.

Thermal Reservoir Temperature

Thermal reservoir temperature is commonly used to classify geothermal system origins and assess resource potential. Primary methods include direct drilling measurements and computational estimations [24]. Due to the high cost of direct drilling, computational methods – commonly referred to as geothermal temperature scales – are generally employed. Researchers widely use four primary geothermal temperature-scale methods: the SiO_2 geothermal scale, the cation geothermal scale, the isotope geothermal scale, and the gas temperature scale. Researchers frequently use the SiO_2 and Na-K-Mg thermometers to characterize geothermal waters.

The SiO_2 geothermal thermometer estimates reservoir temperature by relating dissolved silica concentration in geothermal fluids to reservoir temperature and pressure [24, 25]. Since SiO_2 solubility varies with temperature, its concentration serves as

a reliable indicator of reservoir thermal characteristics. This method is suitable for estimating temperatures between 20 and 250ºC. Different SiO_2 thermometer formulas apply depending on mineral composition and cooling processes. This study employed SiO_2, Na-K, and Na-K-Ca geothermal thermometers to derive geothermal cavity temperatures in the Huitang area. Since all geothermal water temperatures in the study area were below 100ºC and there was no steam loss, the quartz geothermal thermometer method used Eq. (2).

$$T = \frac{1309}{5.19 - \log SiO_2} - 273.15 \quad (2)$$

The Si–Enthalpy model is an essential hydrogeochemical tool in geothermal studies. It is mainly used to estimate geothermal reservoir temperatures and the proportion of cold water mixing. The model, proposed by Truesdell and Fournier [26], examines the relationship between silica (SiO_2) concentration and enthalpy in geothermal fluids [27]. This model can accommodate two scenarios: one with steam loss before cold water mixing and one without [28]. It is used to correct temperature-estimation errors caused by mixing cold and hot water.

The traditional SiO_2 geothermal thermometer underestimates reservoir temperatures under these conditions. To address this limitation, Eq. (3) of the silicic enthalpy method and the graphical silicic enthalpy approach were used to estimate the cold water proportion and the geothermal cavity temperatures.

a) Silicic Enthalpy equation

$$\begin{cases} S_c x + S_h(1-x) = S_s \\ \rho_c(SiO_{2c}) + \rho_h(SiO_{2h})\, SiO_{2h}(1-x) = \rho_s(SiO_{2s}) \end{cases} \quad (3)$$

In the equation, S_c represents the enthalpy of cold water (J/g); S_s represents the final enthalpy of spring water; S_h represents the initial enthalpy of hot water; $\rho_c SiO_2$ represents the SiO_2 concentration of cold water (mg/L); $\rho_h SiO_2$ represents the SiO_2 concentration of spring water; $\rho_s SiO_2$ represents the initial SiO_2 concentration of hot water; x represents the cold water proportion.

b) Silicic acid diagram method

The silicic acid diagram method is a well-established technique for correcting geothermal fluid mixtures. By plotting enthalpy values against SiO_2 concentration, this method provides an intuitive estimate of reservoir temperature [24, 29]. Specifically, the enthalpy and SiO_2 concentration of cold water are plotted at the cold water endpoint (Point A), and those of geothermal water are plotted at the hot water endpoint (Point B). Connecting and extending these two points intersects the quartz dissolution trend at Point C, which represents the corrected reservoir temperature. Researchers calculate the proportion of cold water using the enthalpy difference between cold water and geothermal water. In graphical analysis, based on similar triangles, the ratio is given by (C enthalpy – B enthalpy) / (C enthalpy – A enthalpy).

Circulation Depth

Using the circulation-depth formula (Eq. (4)) [29], the vertical range of fluid circulation of the geothermal water was estimated.

$$H = \frac{t - t0}{\Delta t} + h \quad (4)$$

In this equation, H represents the circulation depth (m); t denotes the calculated thermal reservoir temperature (ºC); t_0 is the constant-temperature zone temperature in the study area; Δt is the geothermal gradient (ºC/100 m); h is the constant-temperature zone depth.

Results

Hydrochemical and Isotopic Characteristics

Statistical analysis of groundwater chemical indicators in the Huitang area reveals (Table 1) that groundwater pH ranges from 6.58 to 8.68. Cold water has a pH range of 7.42 to 7.90, indicating neutral to weakly alkaline water quality. Geothermal water has an average pH of 8.22-8.64, indicating weakly alkaline water quality. The TDS values range from 92.00 to 374.00 mg/L, and the coefficients of variation range from 0.05 to 0.39. These results suggest that the overall water quality in the study area is good and that all samples fall within the freshwater category.

The concentrations of primary cations in different groundwater types, from highest to lowest, were as follows: for cold water, $Ca^{2+}>Na^{+}>K^{+}>Mg^{2+}$, and for geothermal water, $Na^{+}>Ca^{2+}>K^{+}>Mg^{2+}$. The major anions showed the following concentration sequence: in cold water, $HCO_3^{-}>SO_4^{2-}>NO_3^{-}>Cl^{-}$, whereas in geothermal water, $HCO_3^{-}>SO_4^{2-}>Cl^{-}>NO_3^{-}$. Specifically, among groundwater cations, Na^{+} and Ca^{2+} were the primary constituents. Cold water was dominated by Ca^{2+}, with a concentration range of 3.10-89.98 mg/L, while geothermal water was dominated by Na^{+}, with concentrations ranging from 4.61 to 89.62 mg/L. Among anions, HCO_3^{-} exhibits the highest concentration, ranging from 16.10 to 272.34 mg/L. Moreover, the box plots show highly consistent hydrochemical patterns among the groundwater samples in the study area, suggesting that the Huitang geothermal waters share a common recharge source (Fig. 2).

Stable hydrogen and oxygen isotopes (δD and $\delta^{18}O$) and strontium isotopes ($^{87}Sr/^{86}Sr$) were analyzed in geothermal water samples from the Huitang area. The δD values fluctuate between −51.07‰ and −39.76‰,

Table 1. Statistical analysis of hydrochemical and isotopic indicators for geothermal water in the Huitang area.

Groundwater Types	Geothermal water					Cold water				
Statistical Parameters	Max	Min	Mean	Sd	CV(%)	Max	Min	Mean	Sd	CV(%)
K^+	4.43	2.60	3.77	0.74	0.20	35.69	0.81	6.85	7.69	1.12
Na^+	89.62	78.74	85.31	4.91	0.06	65.76	4.61	19.98	11.99	0.60
Ca^{2+}	11.97	3.10	8.15	3.98	0.49	89.98	12.72	48.22	23.05	0.48
Mg^{2+}	0.53	0.04	0.30	0.21	0.71	14.34	0.64	6.52	3.03	0.46
HCO_3^-	162.33	142.21	154.06	8.50	0.06	272.34	16.10	147.65	73.04	0.49
SO_4^{2-}	67.55	4.09	35.62	26.92	0.76	63.26	2.75	29.36	18.51	0.63
Cl^-	6.91	1.72	4.94	2.37	0.48	56.61	2.58	16.50	12.45	0.75
F^-	14.70	4.53	7.85	4.69	0.60	3.46	0.00	0.44	0.75	1.70
NO_3^-	5.05	3.65	4.27	0.46	0.11	47.41	2.29	20.21	11.73	0.58
SiO_2	145.62	97.33	114.76	20.72	0.18	62.47	20.05	40.30	13.01	0.32
TDS	266.00	207.00	234.83	22.68	0.10	374.00	92.00	221.13	82.04	0.37
pH	8.68	8.17	8.36	0.22	0.03	8.01	6.58	7.48	0.37	0.05
Sr	0.13	0.03	0.08	0.04	0.54	0.66	0.06	0.19	0.13	0.67
δD/‰	-39.76	-40.94				-29.93	-36.58			
$\delta^{18}O$/‰	-4.95	-6.31				-5.36	-7.04			
$\delta^{87}Sr/\delta^{86}Sr$	0.723	0.721				0.721	0.713			

indicating a variation in the isotopic composition. The $\delta^{18}O$ values mainly fall between −8.73‰ and −5.63‰. The deuterium excess parameters (d) range from 5.29 to 18.73. The $^{87}Sr/^{86}Sr$ ratios vary from 0.723096 to 0.723725, indicating a relatively narrow isotopic range for strontium in the geothermal waters.

Hydrochemical Chemistry Types

The cation diagram shows that most cold water samples from the Huitang area plot near the Ca^{2+} end-member, indicating a Ca-type composition. The geothermal water samples are mainly located

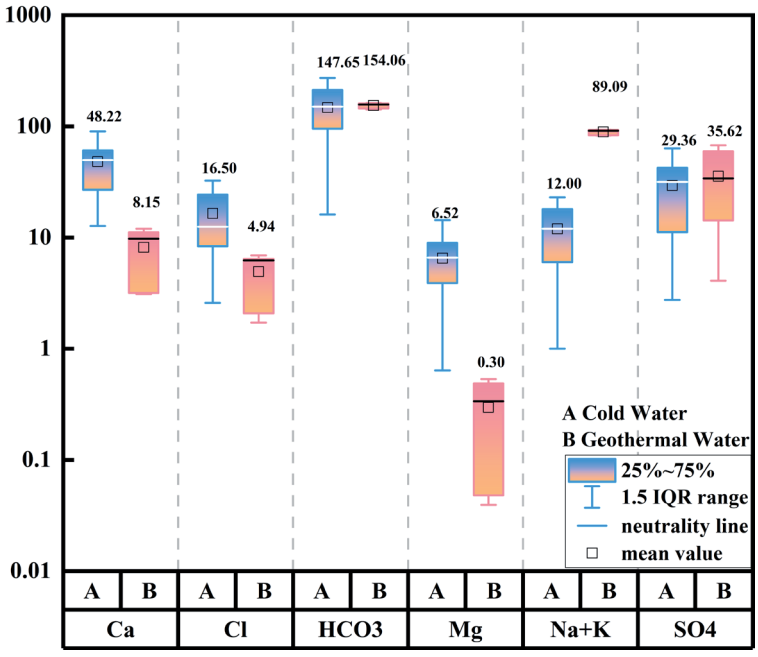


Fig. 2. Box plot of major geochemical components in geothermal water from the Huitang area.

near the $Na^+ + K^+$ end-member, with milliequivalent percentages exceeding 50%, indicating a Na-type composition. These results suggest that Ca^{2+} and $Na^+ + K^+$ are the dominant cations in the groundwater of the study area, whereas Mg^{2+} contributes only a minor proportion. In the anion diagram, groundwater samples cluster near the $HCO_3^- + CO_3^{2-}$ end-member, indicating an HCO_3-type classification. Based on the Shukarev classification system, the groundwater chemistry types in the Huitang area's cold water include HCO_3-Ca, HCO_3-Ca·Na, HCO_3·SO_4-Ca, HCO_3·SO_4-Ca·Na, HCO_3·Cl-Ca·Na, and Cl-Ca·Na. The HCO_3-Ca type predominates, accounting for the most significant proportion. The geothermal water exhibits hydrochemical types HCO_3-Na and HCO_3·SO_4-Na, with HCO_3-Na being the predominant type (Fig. 3). Compared with Zhongshan in Guangdong (HCO_3^--Na·Ca) and Kahui in Sichuan (SO_4^--Na), the Huitang geothermal water displays a distinct hydrochemical type. This difference is mainly controlled by host rock lithology: Huitang is dominated by Yanshanian granites, where the alteration of sodium-rich plagioclase releases Na^+ and HCO_3^-, whereas Kahui is influenced by carbonate rocks, resulting in a higher proportion of SO_4^{2-}.

Discussion

Heat Source Analysis

The geothermal system's heat source acts as the primary force sustaining its energy cycle and is critically important. Under varying geological conditions, the types of internal heat sources within geothermal systems differ. In general, geothermal heat sources derive from two primary sources: thermal energy transmitted from the deep crust and upper mantle, and heat produced by the radioactive decay of elements such as U, Th, and K in the shallow crust, together with thermal input from magmatic fluids [30, 31].

In the Huitang geothermal area, thermal energy transfer from the deep crust and upper mantle occurs primarily through deep major faults. Given the geothermal conditions, deep major fault structures are well developed. The Wujiang Fault and its associated fractured zones host highly permeable lithologies that serve as preferential pathways for groundwater flow. These pathways allow groundwater to penetrate the deep geothermal reservoir and absorb heat, functioning as effective conduits for heat transfer.

Furthermore, the Huitang geothermal system receives supplementary heat from the decay chains of U, Th, and K within the granitic rocks [32]. Studies have analyzed radioactive elements in the Huitang-Weishan granite. They determined average heat generation rates of 3.41 μW/m³ for uranium (U), 3.56 μW/m³ for thorium (Th), and 3.56 μW/m³ for potassium (K). These findings indicate substantial geothermal potential within the Huitang-Weishan granite. Therefore, the Huitang geothermal system is primarily heated by terrestrial heat exchange and the radioactive decay of elements in granite [33]. Additionally, based on Huitang's geological background, multiphase tectonic activity may also convert released stress into thermal energy.

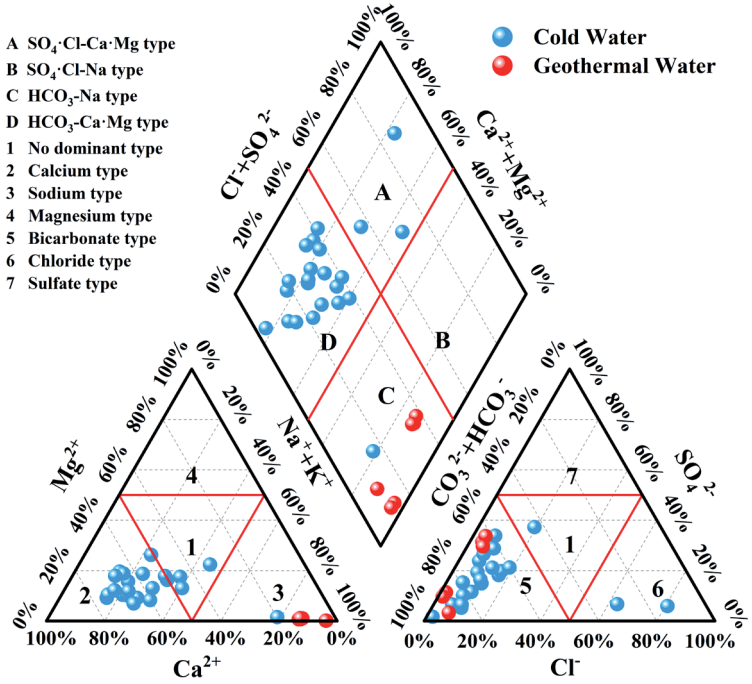


Fig. 3. Piper diagram of geothermal waters from the Huitang area.

Thermal Reservoir Temperature Analysis

Thermal Storage Equilibrium State

The Na-K-Mg ternary diagram shows the equilibrium state between geothermal water and surrounding rocks [34]. It divides geothermal fluids into three types: fully equilibrated water, partially equilibrated water, and immature water [35]. We plotted the Na, K, and Mg concentrations of the groundwater samples on the modified Na-K-Mg ternary equilibrium diagram (Fig. 4). The cold water samples plot near the Mg apex of the Na-K-Mg triangle. The geothermal water plots progressively farther from the Mg apex and align along the transition zone between immature and partially equilibrated waters. This pattern indicates that geothermal water experiences stronger water–rock interaction than cold water. The geothermal water falls within the immature-water field, suggesting that shallow cold water infiltration affects the system. The long-term performance of reinjection wells in the Huitang area indicates that the geothermal system has also been affected by sustained cold water reinjection. Since the immature water zone is susceptible to dilution, cooling, and mixing processes that can shift cation ratios away from equilibrium, the cation thermometer method may not fully reflect the actual reservoir temperatures [24, 26]. Therefore, further analysis is required to determine the thermal energy storage system temperature of the study area's geothermal water.

Thermal Reservoir Temperature Estimation

Using the SiO_2 geothermal thermometer, reservoir temperatures were estimated to range from 135.69 to 140.98ºC. The calculated results were generally lower than those from the Na-K-Mg ternary equilibrium diagram, indicating that cold water recharge primarily influenced the geothermal water. Additionally, mixing with shallow cold water during its ascent further lowered the calculated temperatures.

Analysis of the Na-K-Mg ternary equilibrium diagrams and of SiO_2 geothermal thermometers indicates that ascending geothermal water often mixes with shallow cold water. This mixing lowers the measured spring temperatures relative to the original reservoir temperature [24, 36].

The average cold water temperature in the study area is 17ºC, with an average SiO_2 concentration of 47.7 mg/L. The measured average temperature of geothermal water in the Huitang area was 78ºC, with measured SiO_2 concentrations averaging 140.86 mg/L and 101.71 mg/L.

Substituting these values into the formula yielded a series of X_1 and X_2 values, as shown in Fig. 5a). The geothermal water temperature and the proportion of cold water in the Huitang area were calculated to be 135.69~140.98ºC and 64%, respectively.

The results shown in Fig. 5b) indicate a thermal reservoir temperature of 170ºC and a cold water content of 65% for the study area. Compared with SiO_2 geothermal temperature calculations, the cold water content results are broadly consistent. Since traditional SiO_2 geothermal temperature scales yield lower temperatures due to cold water mixing, the silicic acid diagram method provides calibration. The primary heat sources for the Huitang geothermal field are terrestrial heat flow and heat generated by radioactive decay in granite. Predecessors studied the Weishan granite in Huitang and proposed that the maximum temperature at a depth of 4 km within the Weishan rock mass could reach 178.2ºC. Compared with the calorific storage thermal conditions derived utilizing the SiO_2 geothermal temperature scale, the silicic acid diagram method yields more accurate results.

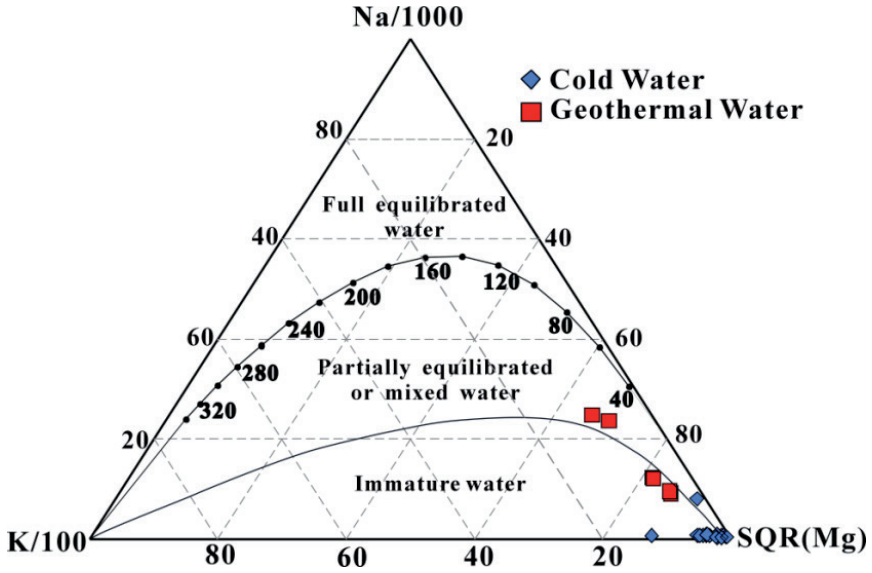


Fig. 4. Na-K-Mg triangular diagram of geothermal waters.

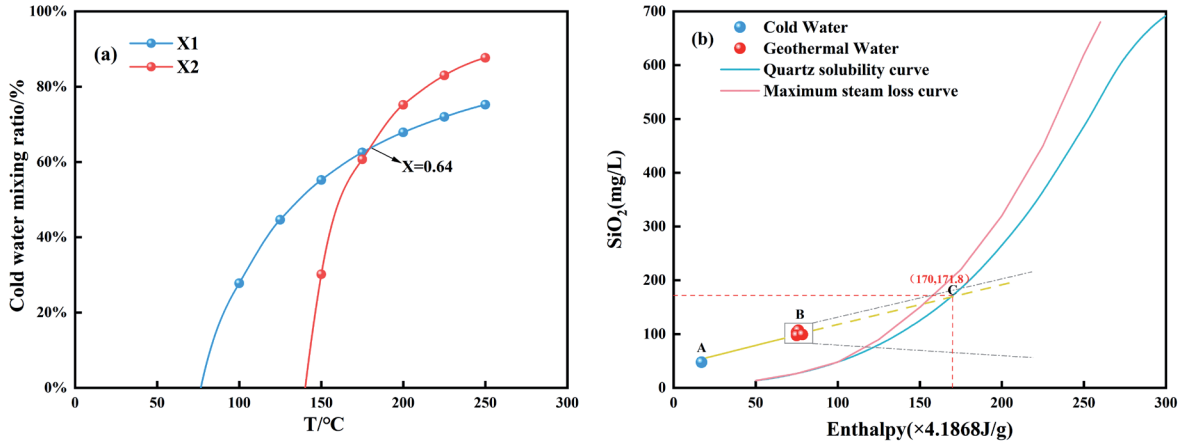


Fig. 5. Silicon-Enthalpy model method diagram of geothermal waters.

Recharge Sources of Geothermal Waters

δD and δ¹⁸O Isotope Analysis

Researchers commonly use stable hydrogen and oxygen isotopes (δD and $\delta^{18}O$) to identify the sources and processes of hydrothermal water recharge. Craig proposed the Global Meteorological Water Line (GMWL: $\delta D = 8\delta^{18}O + 10$) [37]. Since climate and environmental factors influence precipitation across regions, local meteorological water lines (LMWL) should be used for research. Based on prior work, researchers defined the regional meteoric water line (LMWL: $\delta D = 8.41\delta^{18}O + 16.9$). Analysis of the δD–$\delta^{18}O$ diagram (Fig. 6) shows that geothermal water has hydrogen and oxygen isotope compositions similar to those of cold water in the western mountains, indicating a common recharge source. Rainfall, surface water, and groundwater show slopes identical to the local meteoric water line (LMWL). The samples fall near the LMWL, indicating that they mainly originate from meteoric precipitation. This finding is consistent with the box-plot results.

Some surface water samples lie below the LMWL and exhibit negative deuterium excess values, indicating intense evaporation during collection and runoff [7]. Cold water samples are positioned above the LMWL, suggesting that their recharge originates in western,

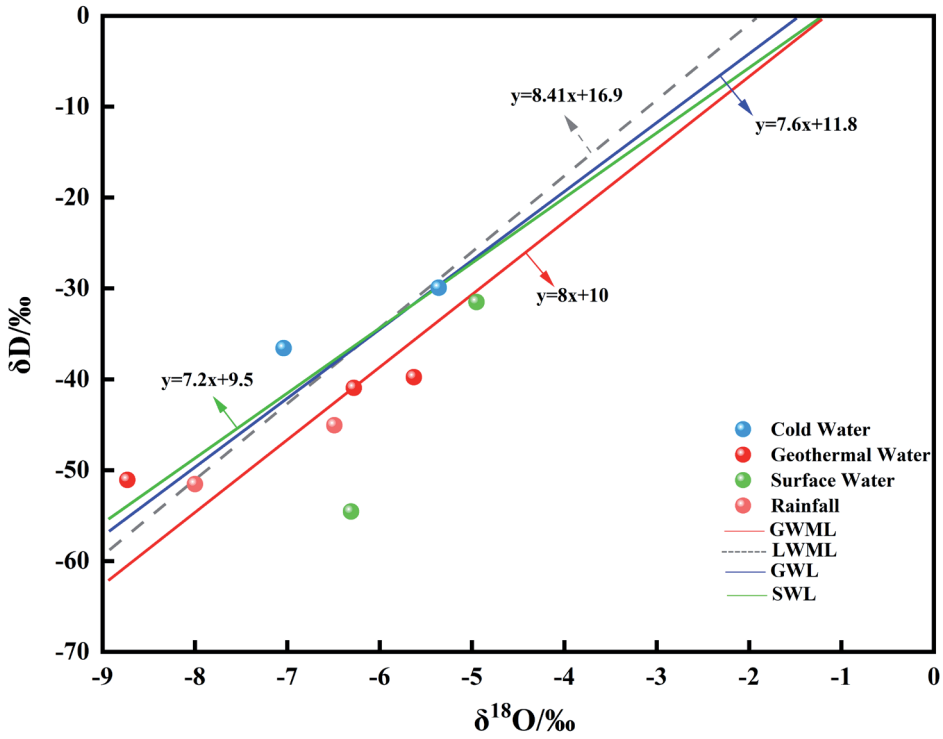


Fig. 6. The δD vs. $\delta^{18}O$ diagram of rainfall, surface waters, and geothermal waters.

higher-elevation mountainous areas. The hydrogen and oxygen isotopic constituents of geothermal water are similar to the isotopic signatures of meteoric precipitation. The isotopic values plot mainly just below the meteoric water line (MWL). A rightward shift is not apparent. The salt content of geothermal water primarily originates from the dissolution of rock minerals. Water–rock isotopic exchange plays only a minor role in the system [29]. Due to the development of faults in the Huitang mining area, geothermal water in the study area is predominantly characterized by the features of deep Yanshanian granites. Local atmospheric precipitation also replenishes groundwater through deep, large-scale faults.

Ion Analysis Based on Gibbs Diagrams

The groundwater chemical Gibbs diagram for the Huitang area shows that the TDS range for geothermal water is 207.00-266.00 mg/L, while that for cold water is 92.00-374.00 mg/L (Fig. 7). The cation-to-anion mass concentration ratios for geothermal water ranged from 0.01 to 0.05 and 0.88 to 0.97. In contrast, those for cold water ranged from 0.01 to 3.52 and 0.14 to 0.82. Most samples plot in the rock-alteration domain, indicating that groundwater composition in the study area is primarily governed by mineral alteration and dissolution within the aquifer. That is, hydrothermal interaction is the primary process for ion sourcing, while evaporation-concentration and atmospheric precipitation contribute minimally to the transport of major ions and have negligible effects. Secondly, some geothermal water samples lie outside the $Na^+/ (Na^+ + Ca^{2+})$ curve, suggesting that factors beyond rock alteration, such as cation adsorption, may influence their hydrochemical composition, consistent with the box plot results.

Hydrothermal Water-Rock Interactions

The ratios of Ca^{2+}/Na^+, Mg^{2+}/Na^+, and HCO_3^-/Na^+ serve as key indicators for evaluating water-rock reactions and interactions [38, 39]. These ratios also enable a qualitative assessment of how the decomposition and dissolution of different rocks influence solute concentrations in hydrothermal water. As shown in Fig. 8, Ca^{2+}/Na^+ ratios in geothermal water samples from the study area predominantly range from 0.03 to 0.14, while Mg^{2+}/Na^+ ratios primarily fall between 0 and 0.01. In contrast, the HCO_3^-/Na^+ ratio predominantly ranges from 1.78 to 1.83. The geothermal water in the Huitang area is mainly distributed near the silicate-rock end-member. A gradual shift toward the carbonate-rock end-member is observed. The composition of geothermal water is primarily governed by the alteration and dissolution of silicate minerals, including feldspar. The alteration and dissolution of carbonate minerals, such as dolomite, also contribute to the overall chemical signature. Furthermore, the Ca^{2+} and Na^+ ions in the geothermal water are shaped by the dissolution of evaporite salts. Still, the contribution from silicate mineral alteration and dissolution is greater than that from carbonate and evaporite dissolution.

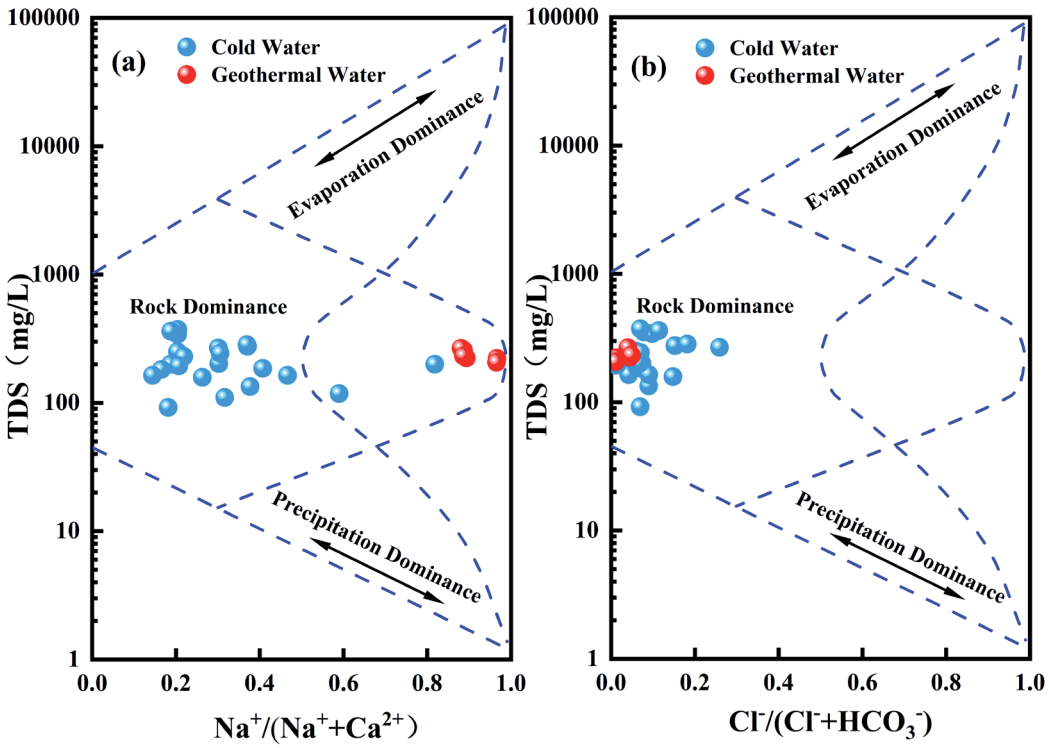


Fig. 7. The Gibbs diagram of geothermal waters: a) ($Na^+/Na^+ + Ca^{2+}$) vs. TDS and b) ($Cl^-/Cl^- + HCO_3^-$) vs. TDS.

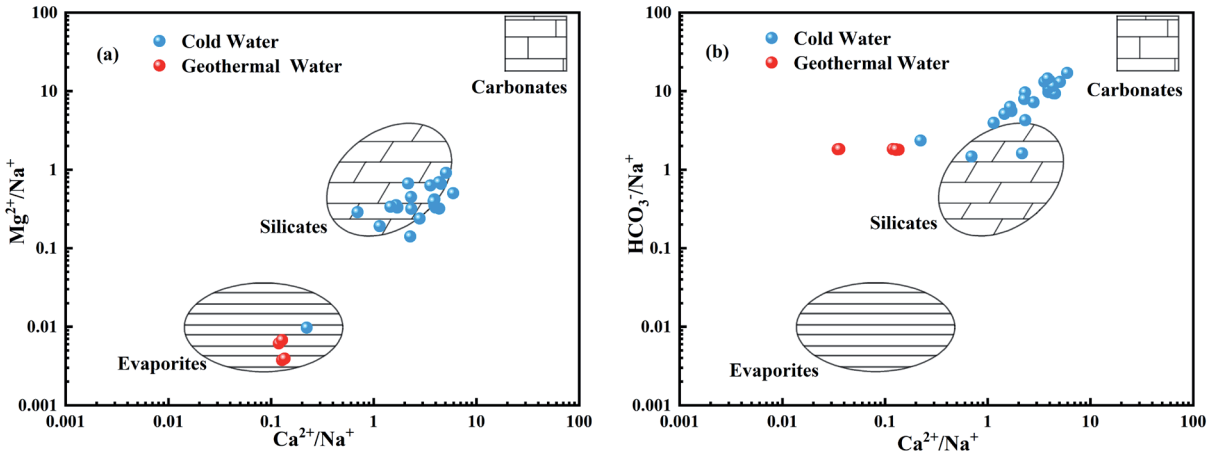


Fig. 8. Hydrothermal water-rock interaction analysis diagram of geothermal water: a) (Ca^{2+}/Na^{+}) vs. (Mg^{2+}/Na^{+}) and b) (Ca^{2+}/Na^{+}) vs. (HCO_3^{-}/Na^{+}).

$\delta^{87}Sr/\delta^{86}Sr$ Isotope Analysis

By measuring the $\delta^{87}Sr/\delta^{86}Sr$ values (Fig. 9), the origin of Sr in geothermal water can be identified [40, 41]. The figure shows that Sr concentrations in geothermal water are mainly due to the dissolution of silicate minerals, consistent with the observed results. The $\delta^{87}Sr/\delta^{86}Sr$ values of geothermal water in the Huitang area are higher than those of cold water, suggesting greater runoff pathways and burial depths for geothermal water. The $\delta^{87}Sr/\delta^{86}Sr$ values of geothermal water show greater similarity to those of cold water from the western mountainous region, suggesting a consistent recharge source for the geothermal water in the Huitang area. Recharge wells may also supply cold water that, through deep circulation pathways, interacts with geothermal water before ascending to the surface along the Wujiang Fault.

To quantitatively evaluate the relationship between strontium isotope characteristics and hydrochemical evolution, we performed a linear regression analysis of $\delta^{87}Sr/^{86}Sr$ versus Na^{+} concentration (Fig. 10) [42]. The data show a highly significant positive correlation ($R^2 = 0.917$, $p<0.001$), which conforms to the equation:

$$\delta^{87}Sr/\delta^{86}Sr=0.7119+1.30\times10^{-4}[Na^{+}] \quad (R^2=0.917, p<0.001) \tag{5}$$

This relationship indicates that the extent of dissolution of sodium-bearing silicate minerals, such as plagioclase, mainly controls the strontium isotope signatures. The cold waters reflect predominantly carbonate-dominated water-rock interactions, whereas the geothermal waters point to intense silicate alteration. These data are consistent with the Gibbs diagram and ion-ratio analyses presented above.

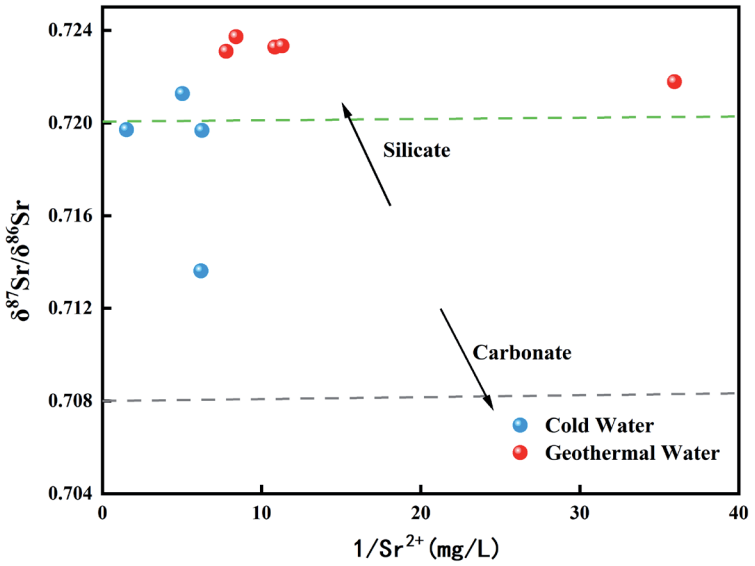


Fig. 9. ($\delta^{87}Sr/\delta^{86}Sr$) vs. Sr diagram of geothermal water.

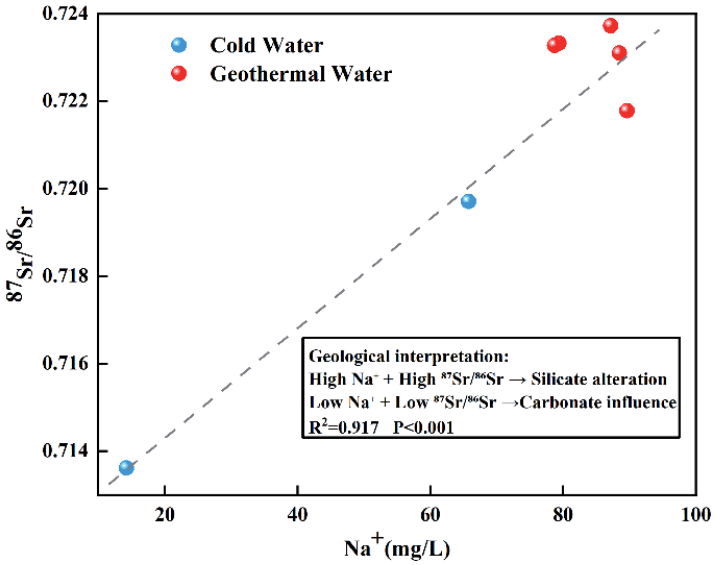


Fig. 10. $\delta^{87}Sr/^{86}Sr$ vs. Na^+ concentration for groundwater samples from the Huitang geothermal area.

Recharge Elevation and Estimation of Circulation Depth

Calculations using the formula indicate that the recharge altitude of geothermal water in the Huitang area ranges from 443.84 to 493.67 m, with a mean value of 468.76 m (Eq. (1)).

Fault structures primarily influence the formation of the Huitang geothermal water. Major deep faults within the area provide favorable thermal pathways for the downward circulation of geothermal water. As a result, atmospheric precipitation is the primary recharge source for geothermal water in the Huitang area. As it infiltrates along these major deep faults, it undergoes heating by the geothermal gradient during deep circulation. In the circulation-depth formula (Eq. (4)), t_0 is taken as the local average air temperature of 17ºC in Huitang, Δt is based on previous studies indicating a gradient of 3.51-4.54ºC/100 m in Ningxiang, with 3.51ºC/100 m adopted, and h is set at 30 m. The vertical range of fluid circulation of the Huitang geothermal water was estimated to be 3411-3562 m. Notably, the circulation depth of the Huitang geothermal water (3411-3562 m) is significantly greater than that of fracture-type geothermal systems along the Guangdong coast. This considerable depth is attributed to the deep-seated faults developed in the Huitang area (e.g., the Wujiang Fault), which provide favorable conduits for deep circulation.

Ion Analysis of Geothermal Water

PC1 and PC2 explain 42.2% and 28.0% of the variance, respectively, enabling analysis of component correlations (Fig. 11a)). The results indicate minimal

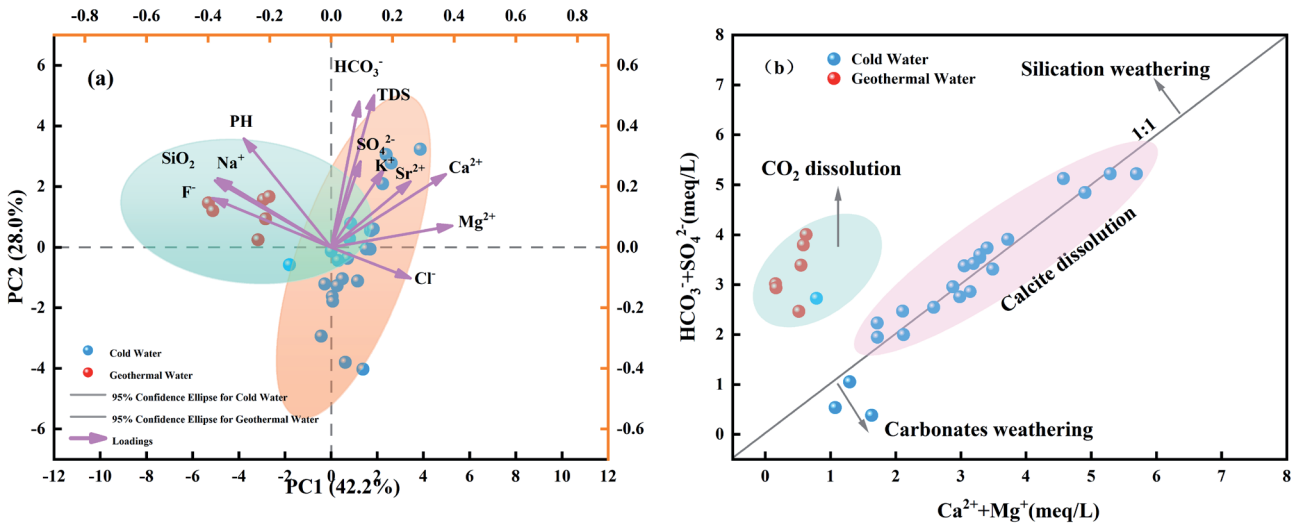


Fig. 11. The PCA diagram a) and (Ca^{2+} + Mg^{2+}) vs. (HCO_3^- + SO_4^{2-}) b) diagram of geothermal water.

variation among samples. The angle between pH and Cl^- exceeds 90°, with a negative cosine value, indicating a negative correlation. The smaller angle between pH and SiO_2 indicates a strong positive correlation, suggesting that silicate dissolution influences pH.

In the $(Ca^{2+} + Mg^{2+}) / (HCO_3^- + SO_4^{2-})$ ratio diagram (Fig. 11b)), the geothermal water samples are mainly plotted above the 1:1 line. The distribution indicates that Ca^{2+} and Mg^{2+} in the geothermal water are derived primarily from the dissolution of silicate minerals [43, 44]. The cold water samples are positioned close to the 1:1 line. The position is interpreted as indicating that the cold water is controlled mainly by the dissolution of carbonate and silicate rocks. Additional evidence is provided for the dominant influence of silicate alteration and dissolution. Cold water in the Huitang area clusters close to the 1:1 line, suggesting that carbonate and silicate dissolution exert primary control, further confirming that it is primarily influenced by silicate alteration [45].

The Na-Cl diagram (Fig. 12a)) shows that the cold water samples are positioned near the 1:1 line. This position is interpreted to indicate that Na and Cl mainly drive halite dissolution in the cold water. The geothermal water samples are located below the 1:1 line. The distribution is interpreted as showing an enrichment of Na^+ relative to Cl^-. The elevated Na^+ levels result from the breakdown of Na-bearing silicate minerals in the geothermal system [46, 47]. Cation-exchange reactions can also increase Na^+ concentrations by replacing Ca^{2+} and Mg^{2+} in water. In Fig. 12b), 99% of the samples show chloro-alkaline indices below zero and fall within the forward cation-exchange zone. The distribution is interpreted as confirming the occurrence of Ca-Na exchange in the geothermal water [48, 49]. Several factors provide support for the interpretation:

a) Cold water carrying CO_2 enters the aquifer from the recharge zone and dissolves in the carbonate rock strata (Eq. (6)), increasing Ca^{2+} concentration.

$$2CaCO_3 + CO_2 + H_2O \rightarrow 2Ca^{2+} + 2HCO_3^- \quad (6)$$

b) When groundwater temperature increases, its dissolution capacity for calcium feldspar and potassium feldspar within rock strata decreases, while its leaching capacity for sodium feldspar correspondingly increases. Ion exchange occurs between Ca^{2+} and Na^+ ions in the geothermal water (Eq. (7)) [50].

$$2R\text{-}Na + Ca^{2+} \rightleftharpoons R_2\text{-}Ca + 2Na^+ \quad (7)$$

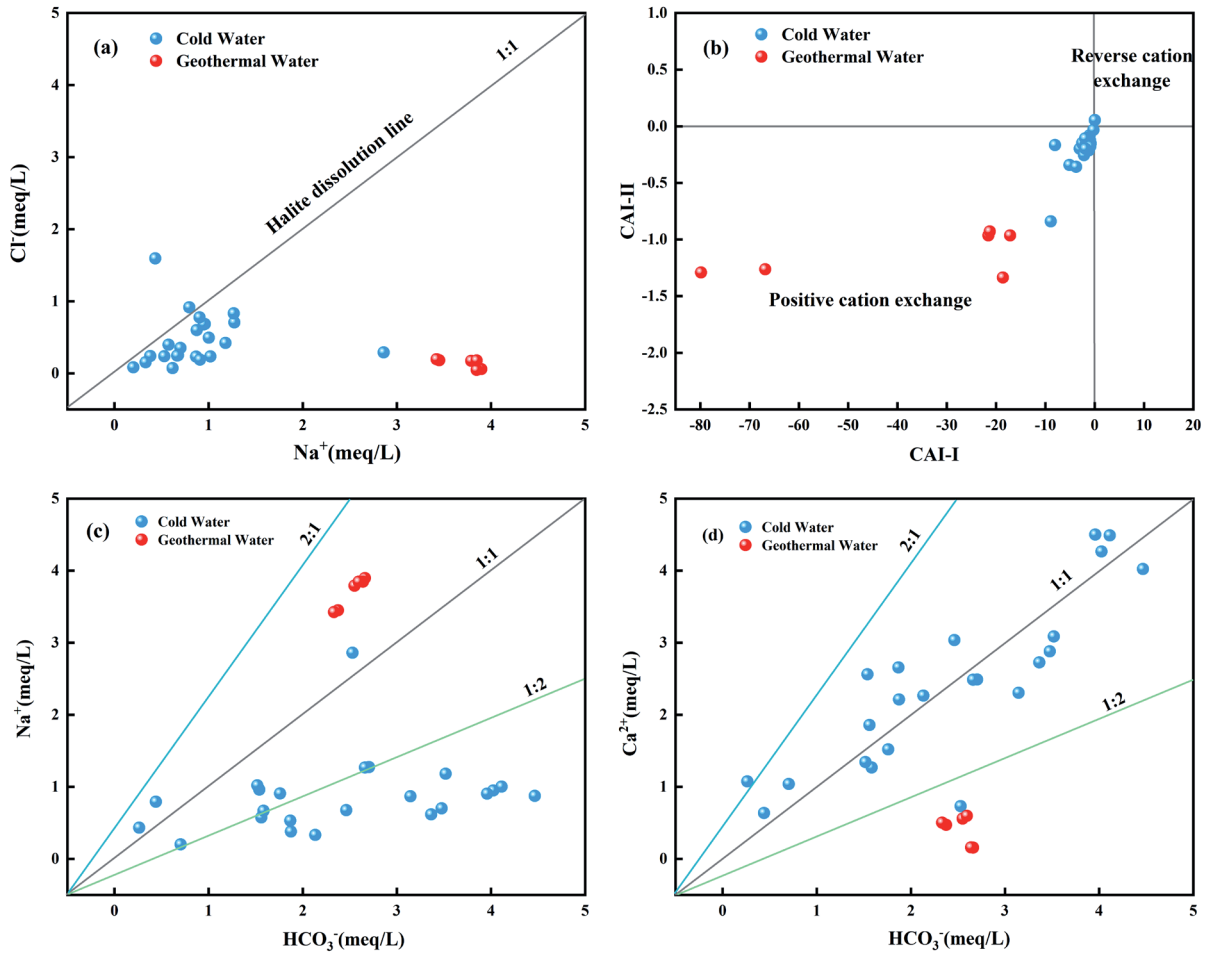


Fig. 12. Hydrochemical analysis diagram of geothermal water: a) Na^+ vs. Cl^-; b) CAI-I vs. CAI-II; c) Na^+ vs. HCO_3^-; d) Ca^{2+} vs. HCO_3^-.

c) Based on actual conditions, the prolonged use of recharge wells to supply tap water in the study area has elevated pH, thereby increasing Na^+ concentration in the geothermal water. In an alkaline environment, plagioclase undergoes dissolution, releasing corresponding Na^+/HCO_3^- and Ca^{2+}/HCO_3^- ions from sodic, anorthic, and calcic feldspars (Eq. (8)).

$$NaAlSi_3O_8 + H_2CO_3 \rightarrow Na^+ + HCO_3^- + Al(OH)_3 + 3SiO_2 \quad (8)$$

Fig. 12c) and Fig. 12d) further illustrate the relationships among Na^+, Ca^{2+}, and HCO_3^-. The Na^+/HCO_3^- relationship diagram shows that geothermal water samples from the Huitang area predominantly exhibit ratios above 1:1 [51]. In contrast, cold water samples primarily fall between 1:1 and 1:2. This indicates that Na^+ in geothermal water samples mainly originates from plagioclase dissolution. In contrast, Na^+ in cold water samples primarily stems from plagioclase dissolution, with natrolite dissolution contributing secondarily. In the Ca^{2+} versus HCO_3^- plot, the cold water samples are positioned above the 1:2 reference line. An excess of Ca^{2+} is indicated. The Ca^{2+} excess is attributed primarily to the dissolution of calcium feldspar. The geothermal water samples plot below the 1:2 line. The position suggests that albite dissolution dominates the composition of geothermal water in the Huitang area.

Genesis Mechanism

The comprehensive review of the above studies provides a more thorough understanding of the geothermal system in the Huitang Geothermal Area. Based on prior research into the geothermal reservoir-forming mechanisms in this region, a genesis model for the Huitang Geothermal Area is presented in Fig. 13. It is evident that the topography rises from the northwest of Huitang toward the Shiziqiao mountainous area. The significant hydraulic head difference provides the driving force for groundwater flow. After being influenced by atmospheric precipitation, cold water infiltrates downward along the F4 fault zone and undergoes dissolution of the host rock in the recharge zone, forming HCO_3^--Ca type groundwater. Subsequently, through deep circulation, it absorbs geothermal and mantle heat, forming geothermal water that then flows southeastward. During this process, cation exchange with silicate rocks occurs, forming HCO_3^--Na type geothermal water. Influenced by the fault zones and aquitards, the geothermal water ascends through

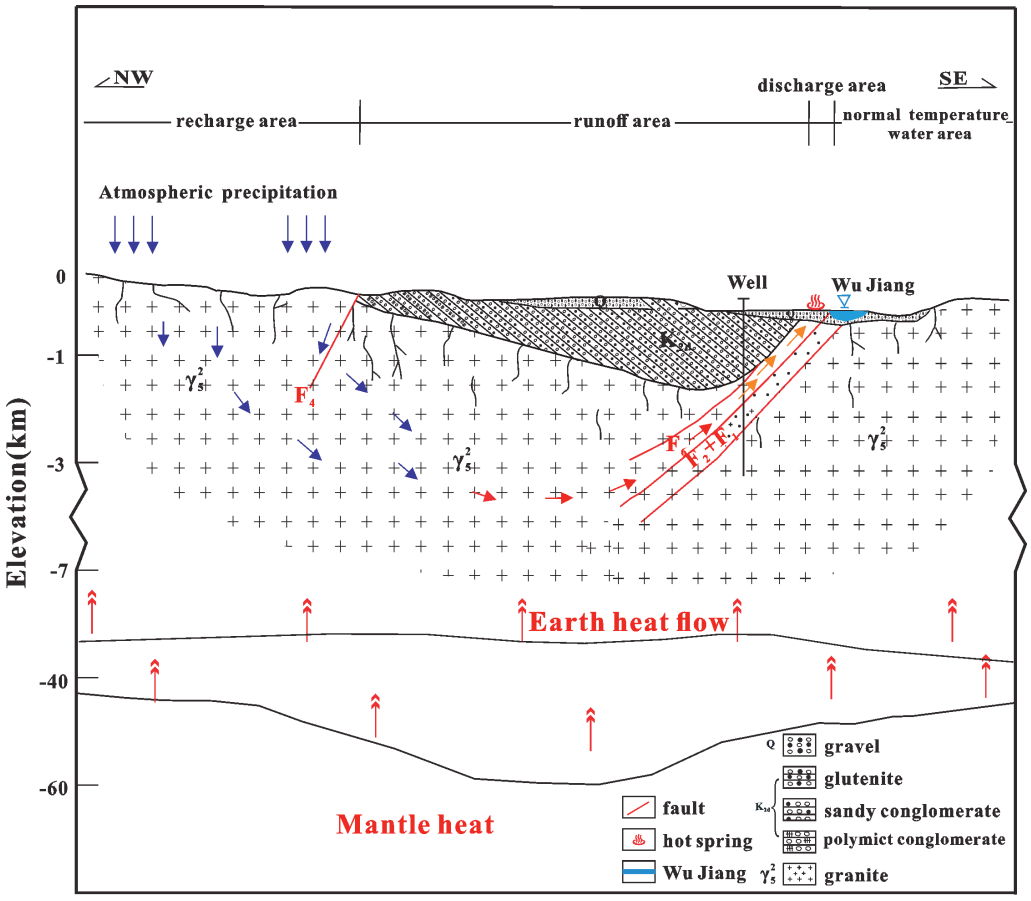


Fig. 13. Conceptual model illustrating the origin of geothermal water in Huitang.

the junction of the F_1 and F_2 faults. During its ascent, it mixes with shallow cold water, markedly decreasing its temperature. In lower-lying areas, it discharges as geothermal water [52].

Conclusions

(1) The primary heat sources of the Huitang geothermal field are terrestrial heat flow and heat produced by the decay of radioactive elements in granite. Multiphase tectonic activity can also convert the released stress into thermal energy. Using the silicic acid equation method and the SiO_2 geothermal temperature scale, the cold water mixing ratio was calculated to be 64%, with a reservoir temperature range of 135.69-140.98ºC. Since the traditional SiO_2 geothermal thermometer yields lower temperatures due to cold water mixing, a correction using the enthalpy diagram method was applied. Verification confirmed that the enthalpy diagram results are more accurate, indicating that the actual thermal reservoir temperature at Huitang is around 170ºC. Stable hydrogen and oxygen isotope (δD and $\delta^{18}O$) diagrams show that atmospheric precipitation is the primary recharge source for the Huitang geothermal water. The estimated recharge elevations range from 443.84 to 493.67 m.

(2) The underground geothermal water in the Huitang area is predominantly neutral to slightly alkaline. Box plots indicate that the primary water chemistry ions are Na^+ and HCO_3^-, classifying the geothermal water as an HCO_3^--Na type. Gibbs diagrams reveal that rock alteration dominates the hydrothermal interactions in the study area. Correlation plots of $(Ca^{2+}/Na^+)/(Mg^{2+}/Na^+)$ and $(Ca^{2+}/Na^+)/(HCO_3^-/Na^+)$, along with strontium isotope ratios ($\delta^{87}Sr/\delta^{86}Sr$), indicate significant dissolution of silicate rocks by the geothermal water.

(3) Based on the above studies, the genesis mechanism of the Huitang geothermal area is constructed as follows: Atmospheric precipitation infiltrates downward along the F4 fault zone, undergoing dissolution with the host rock in the recharge area. Through deep circulation, it absorbs geothermal and mantle heat, forming underground thermal water. The circulation depth of Huitang thermal water ranges from 3411 to 3562 meters. Subsequently, the water flows southeastward. Influenced by the fault zone and aquitards, the geothermal water ascends along the intersection of the F_1 and F_2 faults, discharging as geothermal water.

Acknowledgments

The authors gratefully acknowledge the Hydrogeology and Water Resources Survey Division of the Changsha Center, China Geological Survey, for their valuable guidance during the development of this study. We also appreciate the data support provided by the geothermal resource investigation project team in the Huitang area of Ningxiang City, Hunan Province. In addition, we would like to express our sincere thanks to Haogang Dong, Zhen Xu, and other colleagues from the Hydrogeology and Water Resources Survey Division of the Changsha Center for their thoughtful guidance and assistance in the preparation of this manuscript.

The authors would like to express their sincere appreciation for the support of the following research projects:

Geothermal Resource Investigation Project in the Huitang area of Ningxiang City, Hunan Province (NXCG-F202405200042).

Ecological Restoration Investigation Project in the Huaihua–Shaoyang Region of Southwestern Hunan (DD20230701303).

AI Usage Disclosure Statement

During the preparation of this manuscript, the authors used Grammarly (Grammarly Inc.) and DeepSeek (DeepSeek-AI) for the purpose of English language editing and polishing. After using these tools, the authors reviewed and edited the content as needed and take full responsibility for the content of this publication.

No AI tool was used to generate, interpret, or fabricate any data, results, figures, or scientific conclusions reported in this manuscript.

Conflict of Interest

The authors declare no conflict of interest.

References

1. VACQUIER V. A theory of the origin of the Earth's internal heat. Tectonophysics, **291** (1-4), 1, **1998**.
2. KASSEM M.A., MOSCARIELLO A. Geothermal energy: A sustainable and cost-effective alternative for clean energy production and climate change mitigation. Sustainable Futures, **10**, 101247, **2025**.
3. KALAIR A., ABAS N., SALEEM M.S., KALAIR A.R., KHAN N. Role of energy storage systems in energy transition from fossil fuels to renewables. Energy Storage, **3** (1), e135, **2021**.
4. PANG Z., KONG Y., SHAO H., KOLDITZ O. Progress and perspectives of geothermal energy studies in China: from shallow to deep systems. Environmental Earth Sciences, **77** (16), 580, **2018**.
5. ZHANG J., CHEN L., SUN Y., XU L., ZHAO X., LI Q., ZHANG D. Geothermal resource distribution and prospects for development and utilization in China. Natural Gas Industry B, **11** (1), 6, **2024**.
6. TAYLOR H.P. The application of oxygen and hydrogen isotope studies to problems of hydrothermal alteration and ore deposition. Economic Geology, **69** (6), 843, **1974**.

7. GIGGENBACH W.F. Isotopic shifts in waters from geothermal and volcanic systems along convergent plate boundaries and their origin. Earth and Planetary Science Letters, **113** (4), 495, **1992**.
8. MINISSALE A., EVANS W.C., MAGRO G., VASELLI O. Multiple source components in gas manifestations from north-central Italy. Chemical Geology, **142** (3-4), 175, **1997**.
9. ZHOU X., PENG Y., LI Y., SANG H. Hydrogeochemical evolution, isotopic insights, and genetic models of geothermal water in Anhui province, China. Water, **17** (2), 236, **2025**.
10. SHI X., BAI X., SUN Z., LIU J., YE H., PANG L., CHEN G., YAN H. Hydrochemistry and isotope geochemistry of Bailing geothermal water in northwest Jiangxi: Implications for water-rock interaction. Geothermics, **131**, 103402, **2025**.
11. YIN H., ZHOU W., DONG F., LIU Y., SHI C., MENG M., CHENG W. Hydrochemical characteristics and genetic mechanism of porous sandstone geothermal water in northern Jinan, Shandong, China. Environmental Science and Pollution Research, **31** (16), 24180, **2024**.
12. WANG J. Low-medium temperature geothermal system of convective type. Earth Science Frontiers, **3** (3), 97, **1996** [In Chinese].
13. LI Y., BAI X., HUANG C., CHEN W., MA C., HUANG W., DENG G., QIU X., CHEN S., YANG Y., HUANG Y., WU X., YE H. Genesis of geothermal waters in Zhongshan city, China: Hydrochemical and H-O-C isotopic implications. Water, **16** (13), 1765, **2024**.
14. LIU Z., YE G., WANG H., DONG H., XU B., ZHU H. Geophysics and geochemistry reveal the formation mechanism of the Kahui geothermal field in western Sichuan, China. Minerals, **15** (4), 339, **2025**.
15. HUANG X., ZENG Y., LU S., LU G., OU H., WANG B. Formation and evolution mechanisms of geothermal waters influenced by fault zones and ancient lithology in the Yunkai Uplift, southern China. Water, **17** (13), 1885, **2025**.
16. WAN T. Recent tectonic stress field, active faults and geothermal fields (hot-water type) in China. Journal of Volcanology and Geothermal Research. **22** (3-4), 287, **1984**.
17. OU J., CHEN L., ZHANG B., ZHOU H., TANG X., BAI H., ZHANG D., GAO J. The formation mechanism of the typical hot dry rocks in Hunan Province, China. Journal of Geophysics and Engineering, **19** (6), 1246, **2022**.
18. MOECK I.S. Catalog of geothermal play types based on geologic controls. Renewable and Sustainable Energy Reviews, **37**, 867, **2014**.
19. LIAO D., FENG D., LUO J., YUN X. Relationship between radiogenic heat production in granitic rocks and emplacement age. Energy Geoscience, **4** (4), 100157, **2023**.
20. GIBBS R.J. Mechanisms controlling world water chemistry. Science, **170** (3962), 1088, **1970**.
21. GREENACRE M., GROENEN P.J.F., HASTIE T., D'ENZA A.I., MARKOS A., TUZHILINA E. Publisher Correction: Principal component analysis. Nature Reviews Methods Primers, **3**, 22, **2023**.
22. KHAN F., RAZA A., MAHMOUD M., PATIL S., AL SHAFLOOT T. A comprehensive review of geothermal reservoirs: Current understanding and future outlook. Arabian Journal for Science and Engineering, **50**, 14415, **2025**.
23. DANSGAARD W. Stable isotopes in precipitation. Tellus, **16** (4), 436, **1964**.
24. LIN W., YIN X. Temperature estimation of a deep geothermal reservoir based on multiple methods: a case study in Southeastern China. Water, **14** (20), 3205, **2022**.
25. BIAN K., NIU X., WANG W., WANG X., PANG Y., BALAJI P. Application of geothermal thermometric scale in the study of deep reservoir temperature. Energy Exploration & Exploitation, **38** (6), 2618, **2020**.
26. FOURNIER R.O. Chemical geothermometers and mixing models for geothermal systems. Geothermics, **5** (1-4), 41, **1977**.
27. WANG L., LIU K., ZHANG S., ZHANG Y., JIA W., YU T., GUO J. Estimation of reservoir temperature and analysis of the mechanism of origin of a granite dome-controlled geothermal system in the western Wugongshan area, southeast China. Frontiers in Earth Science, **11**, 1226074, **2023**.
28. GUO Q., PANG Z., WANG Y., TIAN J. Fluid geochemistry and geothermometry applications of the Kangding high-temperature geothermal system in eastern Himalayas. Applied Geochemistry, **81**, 63, **2017**.
29. TIAN J., PANG Z., GUO Q., WANG Y., LI J., HUANG T., KONG Y. Geochemistry of geothermal fluids with implications on the sources of water and heat recharge to the Rekeng high-temperature geothermal system in the Eastern Himalayan Syntax. Geothermics, **74**, 92, **2018**.
30. SUN Y., ZHANG J., XU L., LI J., LI Q., CHEN L., ZHAO X., LI W. Geothermal development model in granite area: a case study of Shangyun area, Yunnan Province, China. Geochemistry International, **62**, 500, **2024**.
31. ZHANG C., FENG Q., ZHANG L., QIN S., JIANG G., HU J., HU S., HUANG R., ZHANG H. Characteristics of radiogenic heat production of widely distributed granitoids in Western Sichuan, Southeast Tibetan Plateau. Lithosphere, **2022** (1), 4165618, **2022**.
32. KADAM A., WAGH V., JACOBS J., PATIL S., PAWAR N., UMRIKAR B., SANKHUA R., KUMAR S. Integrated approach for the evaluation of groundwater quality through hydro geochemistry and human health risk from Shivganga river basin, Pune, Maharashtra, India. Environmental Science and Pollution Research, **29** (3), 4311, **2022**.
33. DONG F., YIN H., YANG Z., ZHOU W., CHENG W., LIU Y. Delineating the controlling mechanisms of geothermal waters quality and suitability zoning in the Lower Yellow River Basin, China. Environmental Technology & Innovation, **38**, 104126, **2025**.
34. HAN S., NAN D., LIU Z., GESANG N., BIANMA C., ZHAO H., ZHENG Y., XIAO P. Hydrochemical characteristics and formation mechanism of geothermal fluids in Zuogong County, Southeastern Tibet. Water, **16** (19), 2852, **2024**.
35. WANG X., YAN X., ZHANG W., MA B., LIU C., YANG Y., YUAN R., CHEN J., SU W. Hydrogeochemical characteristics and evolutionary mechanisms of the Nanping geothermal field, Southeastern Hainan Island, China. Sustainability, **17** (13), 6189, **2025**.
36. LI N., ZHOU H., WEN Z., JAKADA H. Formation mechanism and mixing behavior of Nanyang thermal spring, Xingshan County of Hubei Province, central China. Hydrogeology Journal, **27** (8), 2933, **2019**.
37. CRAIG H. Isotopic variations in meteoric waters. Science, **133** (3465), 1702, **1961**.
38. AHMAD I., KHAN S.A., SHOEB M., ISLAM S., KHAN M.A. Hydrochemical facies distribution, controlling mechanisms and natural background concentrations of major pollutants in Ganga-Yamuna interfluve aquifer, India. Environmental Pollution, **368**, 125694, **2025**.

39. MOHAMED A., ASMOAY A., ALSHEHRI F., ABDELRADY A., OTHMAN A. Hydro-geochemical applications and multivariate analysis to assess the water–rock interaction in arid environments. Applied Sciences, **12** (13), 6340, **2022**.
40. WANG Z.-L., ZHANG J., LIU C.-Q. Strontium isotopic compositions of dissolved and suspended loads from the main channel of the Yangtze River. Chemosphere, **69** (7), 1081, **2007**.
41. SHOEDARTO R.M., TADA Y., KASHIWAYA K., KOIKE K., ISKANDAR I., MALIK D., BRATAKUSUMA B. Investigation of meteoric water and parent fluid mixing in a two-phase geothermal reservoir system using strontium isotope analysis: A case study from Southern Bandung, West Java, Indonesia. Geothermics, **94**, 102096, **2021**.
42. HU H., LU G., LU Q., LI Y., XIE L., LIN X., WU M., MO C., ZHANG B. Hydrogeochemical characteristics and geothermometry of hot springs in the tensile tectonic region Leizhou Peninsula and Hainan Island in South China. Geofluids, **2022** (1), 1101015, **2022**.
43. WANG Q., ZHOU D., LIAO J., LIU Y., WANG X. Reservoir temperature calculation and modeling for convective geothermal systems: case study of five major hot springs in Lushan, Henan, China. Geofluids, **2023** (1), 7149973, **2023**.
44. LEI Y., ZHAO Z., QIN G., BA R., YANG S., SHI H. Hydrogeochemical and isotopic analysis for interpreting the formation of the complex geothermal system in the Guide Basin, Northeastern Tibetan Plateau. PLoS One, **20** (2), e0317694, **2025**.
45. WANG Y., YUAN X., ZHANG Y., ZHANG X., XIAO Y., DUO J., HUANG X., SUN M., LV G. Hydrochemical, D–O–Sr isotopic and electromagnetic characteristics of geothermal waters from the Erdaoqiao area, SW China: Insights into genetic mechanism and scaling potential. Ore Geology Reviews, **158**, 105486, **2023**.
46. XU C., XIA B., DONG L., BAI X., WANG X., XIE Y., YU S., LIU H. Hydrogeochemical characteristics and formation mechanisms of groundwater around Ji'an city, Southern China. Sustainability, **17** (22), 10306, **2025**.
47. SUN M., ZHANG X., YUAN X., YU Z., XIAO Y., WANG Y., ZHANG Y. Hydrochemical characteristics and genetic mechanism of geothermal springs in the Aba Area, Western Sichuan Province, China. Sustainability, **14** (19), 12824, **2022**.
48. ZHANG J., CHEN L., HOU X., LIN M., REN X., LI J., ZHANG M., ZHENG X. Multi-isotopes and hydrochemistry combined to reveal the major factors affecting Carboniferous groundwater evolution in the Huaibei coalfield, North China. Science of the Total Environment, **791**, 148420, **2021**.
49. KAI B., HUI S., GUILEI H., HAO Y., JUNPENG Y., XI C. Hydrogeochemical modeling of karst groundwater in the Fengfeng mining area. Water Resources, **50** (6), 948, **2023**.
50. XU J., YUAN G., CAO Y., JIN Z., LIU K. Feldspar dissolution rates and controlling factors under near-equilibrium conditions in subsurface settings. Science China Earth Sciences, **68** (8), 2558, **2025**.
51. ZHENG Y., NAN D., LIU Z., ZHAO H., ZHU M., XING Y., ZENG Q., ZHANG L., HU Z. A conceptual model of the hydrochemical evolution and hydrothermal genetics of the geothermal waters of the Ngari Prefecture, Tibet. Geothermal Energy, **13**, 38, **2025**.
52. YIN H., ZHANG C., ZHOU X., CHEN T., DONG F., CHENG W., TANG R., XU G., JIAO P. Research on the genetic mechanism of high-temperature groundwater in the geothermal anomalous area of gold deposit — application to the copper mine area of Yinan gold mine. ACS Omega, **7** (47), 43231, **2022**.